ATLAS NOTE

ATLAS-CONF-2010-079

20th August, 2010

Early supersymmetry searches in events with missing transverse energy and b-jets with the ATLAS detector

ATLAS collaboration

ATLAS-CONF-2010-079
11 October 2010

Abstract

This note describes a first set of measurements of supersymmetry-sensitive variables in heavy-flavour enriched final state events with jets and missing transverse energy, from initial $\sqrt{s} = 7$ TeV proton-proton collisions at the LHC. Events may contain identified leptons (electron, muon) while separate analyses are carried out considering the no-lepton case and the case with additional leptons. The measurements are based on 305 nb^{-1} of data collected with the ATLAS detector. General good agreement is found between data and Standard Model expectations estimated with Monte Carlo simulations.

1 Introduction

Supersymmetry (SUSY) [1] is one of the most compelling theories to describe physics beyond the Standard Model. If supersymmetric particles are present at the TeV-scale, the production of squarks ($\tilde{q}$) and gluinos ($\tilde{g}$), superpartners of quarks and gluons and therefore strongly interacting particles, constitutes one of the most promising channels for SUSY discovery at the Large Hadron Collider (LHC) [2]. In the framework of minimal supersymmetry (MSSM), the production of third generation squarks could be favoured, as the large mixing between the chiral states of the super-partners of the Standard Model fermions might yield low masses for the lightest scalar bottom and scalar top states. In *R*-parity conserving SUSY scenarios, the cascade decay of pair-produced gluinos and squarks into quarks and gluons will result in a final state consisting of several jets plus missing transverse energy, coming from the undetected neutralinos, which are the lightest supersymmetric particles (LSP) in a large variety of models.

At the LHC, SUSY sparticles such as scalar bottom and scalar top are expected to be produced in pairs (direct production), or through $\tilde{g} \to \tilde{b}b(\tilde{t}t)$ decays if $m_{\tilde{g}} > m_{\tilde{q}} + m_q$. Figure 1 illustrates two possible production mechanisms. Direct pair production of sbottom quarks can lead to a final state consisting of a pair of acoplanar bottom-quark jets (*b*-jets) and significant $E_{\mathrm{T}}^{\mathrm{miss}}$; in case of gluino pair production, multi-jet final states are expected and *b*-jets would be copiously produced in the decay chain. Depending on the sparticle mass spectrum, leptons might also be present.

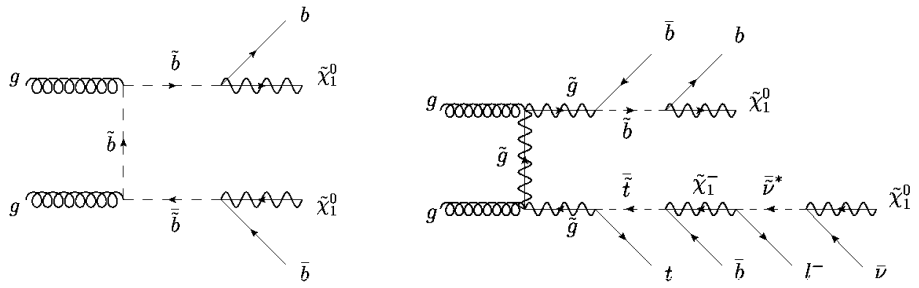

Figure 1: Feynman diagrams of two possible production mechanisms and subsequent decay chain involving third generation squarks: sbottom pair production and sbottom decay into *b*-quark and neutralinos (*left*); gluino pair production and decay into $\tilde{b}b$ and $\tilde{t}t$ (*right*).

The ATLAS collaboration has already reported the observation of the $W^{\pm}$ and Z bosons [3] and of high transverse-momentum jets [4]. With increasing integrated luminosities it is expected that the LHC experiments should soon be reaching sensitivity for the discovery of supersymmetric particles [5] exceeding that of experiments at the Tevatron [6] [7] [8]. First comparisons of data to Monte Carlo simulations for some of the most important kinematic variables for supersymmetry searches involving jets, leptons and missing transverse momentum have already been reported [9] [10].

This note presents a first comparison of data to Monte Carlo simulations for some of the most important kinematic variables for supersymmetry searches involving *b*-jets and missing transverse energy, with and without leptons. The identification of jets which originated from *b*-quarks (*b*-tagging) is based on the presence of a displaced vertex due to the decay of a *b* hadron inside the jet. At least one *b*-jet candidate is required in the event selection. The measurements in this note are based on data collected in proton-proton collisions at $\sqrt{s} = 7$ TeV at the LHC from March to July 2010. They correspond to a total integrated luminosity of 305 nb^{-1}.

2 The ATLAS Detector

A detailed description of the ATLAS detector can be found in [11]. This analysis uses almost all detector components and the following provides a brief summary.

At the core of the ATLAS detector is the inner tracking detector, which is immersed in a 2 T axial field. Silicon pixel and micro-strip detectors provide measurements of charged particle trajectories in the pseudo-rapidity [1] range $|\eta| < 2.5$, complemented by a straw tube tracker for $|\eta| < 2.0$ which enhances electron identification through detection of transition radiation.

Surrounding the solenoidal magnet is the ATLAS calorimetry, covering $|\eta| < 4.9$. The liquid argon (LAr) electromagnetic calorimeter is divided into a barrel ($|\eta| < 1.475$) and two endcaps ($1.375 < |\eta| < 3.2$). The surrounding hadronic tile calorimeter is similarly divided into a barrel ($|\eta| < 1.0$) and two extended barrels ($0.8 < |\eta| < 1.7$). This is complemented by a LAr hadronic endcap calorimeter consisting of two independent wheels per endcap, located behind the electromagnetic endcaps at $1.5 < |\eta| < 3.2$. Forward calorimeters cover the region $3.1 < |\eta| < 4.9$. They consist of three modules: the first is made of copper-LAr and is optimized for electromagnetic measurements; the other two are made of tungsten-LAr and measure primarily the energy of hadronic interactions.

The muon spectrometer is composed of separate trigger and high-precision tracking detectors immersed in a toroidal field provided by three air-core super-conducting magnets. Resistive plate chambers ($|\eta| < 1.05$) and thin-gap chambers ($1.05 < |\eta| < 2.4$) provide trigger information in the barrel and endcap regions, respectively. Monitored drift tubes provide precision measurements of muon tracks over $|\eta| < 2.0$, with the cathode strip chambers covering $2 < |\eta| < 2.7$.

3 Data Sample and Trigger Selection

The data sample presented in this paper was recorded during LHC stable-beam conditions. Only periods when all detector components relevant for this analysis were fully operational and with their nominal settings are considered. After the application of basic data-quality criteria the selected data sample corresponds to an integrated luminosity of 305 nb^{-1}. The uncertainties on the luminosity have been estimated to be $\pm 11\%$ [12].

3.1 Trigger Selection

Different trigger selections are used for each of the channels and efficiencies have been studied. Here, a brief description of the trigger performance in each case is given.

0-lepton channel In the 0-lepton channel, calorimeter-based triggers are used to select events with high transverse momentum jets. To maximize the number of selected events (and thereby reduce statistical uncertainties), the lowest unprescaled transverse momentum trigger is used. In this period of data-taking it is achieved with the $p_{\text{T}} > 15$ GeV level-1 (L1) trigger, where the jet transverse momentum is measured at the electromagnetic (EM) scale, as described in

[1] The right-handed coordinate system employed by ATLAS has the nominal interaction point as its origin. The anti-clockwise beam direction defines the positive z-axis, with the polar angle θ being measured with respect to this axis; pseudo-rapidity is defined as $\eta = -\ln\tan(\theta/2)$. The x-axis points towards the centre of the LHC ring, y points vertically upwards and the azimuthal angle ϕ in the $x-y$ plane is positive for positive y. Transverse components of momentum (p_{T}), energy (E_{T}) and missing energy ($E_{\text{T}}^{\text{miss}}$) are defined in this plane.

Section 5.1. Higher level triggers, at level-2 (L2) and event filter (EF), were operated in pass-through mode, i.e. all events selected by the L1 trigger were accepted. The efficiency has been measured with data relative to the minimum bias trigger and compared to the Monte Carlo trigger simulation [13]. For the kinematic range in jet transverse momentum considered in this analysis, the trigger selection efficiency is above 99%. The trigger efficiencies in data and simulation agree to better than 1%.

Electron channel The electron channel uses events selected primarily by the L1 calorimeter trigger requiring electromagnetic objects with p_{T} >5 GeV (`L1_EM5`), which uses the information provided by the trigger towers in the electromagnetic calorimeter of dimension $\Delta\phi \times \Delta\eta = 0.1 \times 0.1$. In order to further reduce the rate, events are also required to pass a high-level trigger chain (`EF_g10_loose`) selecting electromagnetic objects with transverse energy above 10 GeV at the EM scale in the region of interest indicated by the L1 trigger. The combined efficiency of the trigger chain has been measured from independently triggered events. This efficiency is found to be constant within uncertainties for electrons with $p_{\mathrm{T}} > 15$ GeV and equal to (100^{+0}_{-10})%. The corresponding efficiency from Monte Carlo simulation was found to be (96 ± 3)%, in good agreement with data.

Muon channel The muon channel uses events selected by the L1 trigger `L1_MU6`, which selects events with a hit pattern in the muon chambers consistent with a track with transverse momentum above 6 GeV in the region $|\eta| < 2.4$. The trigger efficiency has been measured [10] using independently triggered events containing one muon with p_{T} >20 GeV, as for the selection used in this analysis described in Section 5.3. For $p_{\mathrm{T}} > 10$ GeV, it is measured to be (73±5)% in the region $|\eta|$ <1.05 and (82±4)% in the region 1.05< $|\eta|$ <2.4, in agreement with Monte Carlo predictions. The efficiency becomes constant within statistical uncertainties for muons with p_{T} above 10 GeV.

4 Monte Carlo Simulation

The data analyzed in this paper are compared with the expectations from Monte Carlo simulations of signal and background processes. Generated events are passed through a full GEANT4 [14] simulation of the ATLAS detector and are reconstructed using the same analysis chain as the data [15]. The Monte Carlo samples considered in this study are listed in Table 1, together with the corresponding cross sections of the processes. A detailed description of the samples is given in the following.

QCD multijet production Large samples of QCD multijet events have been generated using the `PYTHIA` 6.4.21 [16] program, which calculates $2 \rightarrow 2$ matrix elements at leading order in the strong coupling constant. The ATLAS MC09 tune settings described in [17] have been employed. Additional initial and final state radiations are generated by a parton shower algorithm in the leading logarithm approximation. The modified MRST 2007 LO* parton densities [18] are used as input and five flavours are included, with top quarks being modelled via a dedicated generator (see below). The simulated QCD multijet samples are normalized to data in dijet control regions as described in Section 7.2. For the single-muon channel, special muon-filtered QCD Monte Carlo samples have been used to reduce the statistical uncertainties. These samples are equivalent to the generic QCD multijet samples but with a filter applied requiring a muon with $p_{\mathrm{T}} > 10$ GeV and $|\eta|$ <2.8 in the event record before detector simulation.

Physics process	Cross-section × BR (nb)
QCD Multijet ($\hat{p}_T > 8$ GeV)	10.57×10^6
$W \to \ell\nu$(+jets)	31.4
$Z \to \nu\bar{\nu}$(+jets)	5.82
$Z \to \ell^+\ell^-$(+jets)	2.97
$t\bar{t}$	0.164
Single top	0.076
SU4 SUSY point	0.060

Table 1: Cross sections of the Standard Model and SUSY benchmark Monte Carlo samples used in this analysis. $\hat{p}_T$ is the transverse momentum of the two partons involved in the hard-scattering. The cross sections reported are given at NNLO for $W \to \ell\nu$, $Z \to \ell^+\ell^-$ and $Z \to \nu\bar{\nu}$, at NLO+NLL for $t\bar{t}$, at NLO for single top and at leading order for QCD multijet. The cross section for the SU4 point is given at NLO.

Additional samples for QCD multijet processes, simulated with the leading order ALPGEN Monte Carlo program [19], have been used to verify the PYTHIA modeling. The generated events are interfaced with the HERWIG [20] model of hadronisation and the JIMMY [21] model of the underlying event. The CTEQ6L1 [22] parton distribution functions (PDF) are used. At this stage of the analysis, differences between PYTHIA and ALPGEN simulations are within experimental uncertainties, and PYTHIA is adopted as default.

W / Z + jets production The production of W or Z bosons in association with jets is simulated with the ALPGEN Monte Carlo program, chosen because of its ability to model multi-parton final states, with CTEQ6L1 PDFs. Up to five partons are generated in slices of $\hat{p_T}$, the transverse momentum of the hard process. The generated events are interfaced to HERWIG and JIMMY for final state parton showers and underlying event simulation, respectively. The samples are normalized to the integrated luminosity using the cross sections shown in Table 1, based on Next-to-Next-to-Leading Order (NNLO) QCD calculations from the FEWZ program [23].

Top production Top production includes pair and single top processes. In both cases, events are generated using the MC@NLO program [24] which includes full next-to-leading order corrections to the matrix element for the hard process. Final state parton showers and the underlying event are simulated via interfaces to HERWIG and JIMMY, respectively. A top mass of 172.5 GeV is assumed. The $t\bar{t}$ cross section is normalized to the Next-to-Leading Order (NLO) result including next-to-leading-log resummation corrections (NLO+NLL) [25]. The CTEQ6.6 NLO parton set is used in both single and pair top samples for the matrix element, the parton shower and the underlying event.

SUSY signal Expected events and kinematic distributions are compared for illustrative purposes to the prediction from a supersymmetric benchmark scenario in the minimal model of supergravity (mSUGRA). Events are generated using HERWIG++ [26] according to the mass spectrum and branching ratios calculated by ISAJET [27] for the parameters of this point in

mSUGRA space (referred to as SU4). The parameters[2] at the grand unification (GUT) scale are $m_0 = 200$ GeV, $m_{1/2} = 160$ GeV, $A_0 = -400$ GeV, $\tan\beta = 10$ and $\mu > 0$. This point lies in a region of parameter space that is just outside the exclusion of the Tevatron experiments [6]. The squark masses are degenerate for the first and second generation and are predicted to be 410 GeV. The gluino mass is 420 GeV. The lightest squarks are predicted to be the lightest scalar bottom and scalar top quarks ($\tilde{b_1}$ and $\tilde{t_1}$) with masses of 361 GeV and 196 GeV, respectively. The MRST 2007 LO* parton densities are used. The inclusive SUSY production cross section is calculated at leading order by `HERWIG++` to be 42.3 pb, and using `PROSPINO` [28] at next-to-leading order to be 59.9 pb.

5 Lepton, Jet, b-jet and $E_{\mathrm{T}}^{\mathrm{miss}}$ Reconstruction

The final state topologies expected from the production of squarks and gluinos and their subsequent decays are dominated by jets and missing transverse energy. In addition, depending on the SUSY parameters, the presence of leptons in the final state due to intermediate charginos and neutralinos in the cascade decay processes is also possible. To select b-jets final states, the Secondary Vertex SV0 [29] b-tagging algorithm based on the reconstruction of secondary vertices within the jet cone is employed. In order to classify events in different exclusive channels, the same object definition and identification criteria are used in the 0-lepton and 1-lepton channel analyses.

5.1 Object Selection

The following object selections define the particle candidates used in the analyses. These criteria are similar to those used in Ref. [5] but have been further refined to improve the rejection of non-collision backgrounds and to reduce possible undesired detector effects.

Jets are reconstructed using the anti-k_t algorithm [30] with four-momentum recombination and distance parameter $R = 0.4$ (in η–ϕ space) which is appropriate for the typical large jet multiplicity of supersymmetric events. Inputs to the jet algorithm are topological clusters in the calorimeters, measured at the electromagnetic scale. The EM scale does not account for instrumental (detector) effects, such as calorimeter non-compensation and energy losses in inactive regions of the detector, and for inefficiencies in clustering and jet reconstruction. Jets are therefore calibrated to the hadronic energy scale using p_{T} and η dependent correction factors obtained from simulation [31].

A small fraction of jets result from calorimeter noise, out-of-time energy depositions in the calorimeters, or from cosmic ray energy deposits. These misidentified jets have different properties compared to real jets arising from parton fragmentation. A set of requirements (referred to as 'clean up cuts') has been identified in dedicated studies [32] to ensure a good quality of the reconstructed jets. Jets are considered to be misidentified (or low quality) if at least one of the following criteria is fulfilled.

- The fraction of jet energy in the hadronic endcap calorimeter is larger than 0.8 and the number of calorimeter cells containing 90% of the jet energy is less than 6.

[2] In mSUGRA, the mass spectrum of sparticles is determined by five parameters: the common scalar and gaugino masses at the GUT scale, m_0 and $m_{1/2}$, respectively; the common trilinear coupling at the GUT scale, A_0; the sign of the Higgsino mixing parameter, μ; and the ratio of the Higgs vacuum expectation values, $\tan\beta$.

- The fraction of the energy in the hadronic endcap is greater than $1-Q$, where Q is a quality factor based on the signal pulse shape.
- The electromagnetic energy fraction is larger than 0.95 and the pulse shape is very inconsistent with the reference shape ($Q > 0.8$).
- The jet timing differs by more than 50 ns from the expected value for particles from collisions.

The fraction of events containing at least one misidentified jet with $p_{\mathrm{T}}^{\mathrm{EM}}$>10 GeV and $|\eta| < 4.9$ is 5×10^{-5}. These events are removed from the analyses. No additional cuts are applied to remove possible remaining non-collision backgrounds, as these are suppressed by the event selections described in Section 6.

The event pre-selection requires two jets with $p_{\mathrm{T}} > 20$ GeV and $|\eta| < 2.5$. Any jets passing this loose selection are considered when applying the object identification described in Section 5.2. Higher p_{T} cuts are required for jets entering the final selections described in Section 6.

Electrons are reconstructed by algorithms that provide good discrimination between isolated electrons and misidentified hadronic jets. Medium-purity selections based on calorimeter shower shape variables combined with track information are used. Electrons are required to have $p_{\mathrm{T}} > 10$ GeV and $|\eta| < 2.47$. Events with electron candidates pointing to the calorimetric regions around the transition between the barrel and the endcap ($1.37 < |\eta| < 1.52$) are removed. In the following, this selection is referred to as 'electron fiducial cut'. In addition, electrons are required to be isolated, that is the calorimeter transverse energy around the electron within a cone of $\Delta R = \sqrt{\Delta\phi^2 + \Delta\eta^2} = 0.2$ should be less than 10 GeV.

Muons are reconstructed by an algorithm which performs a statistical combination of a stand-alone track reconstructed in the muon spectrometer with a matched track in the inner detector. Muons are required to have $p_{\mathrm{T}} > 10$ GeV and $|\eta| < 2.4$. The association between the stand-alone and inner-detector tracks is performed using a χ^2-test defined from the difference between the respective track parameters weighted by their combined covariance matrices. A χ^2 less than 100 is required for muon candidates in this analysis. To ensure isolation, the energy deposition in the calorimeter in a cone of radius $\Delta R = 0.2$ around the muon track is required to be less than 10 GeV.

Missing Transverse Energy ($E_{\mathrm{T}}^{\mathrm{miss}}$) , also referred to as missing transverse momentum, is computed from calorimeter cells belonging to topological clusters at the electromagnetic energy scale [33]. The transverse missing momentum (x,y) components and $E_{\mathrm{T}}^{\mathrm{miss}}$ are defined by

$$E_x^{\mathrm{miss}} \equiv -\sum_{i=1}^{N_{\mathrm{cell}}} E_i \sin\theta_i \cos\phi_i, \quad E_y^{\mathrm{miss}} \equiv -\sum_{i=1}^{N_{\mathrm{cell}}} E_i \sin\theta_i \sin\phi_i$$

$$E_{\mathrm{T}}^{\mathrm{miss}} \equiv \sqrt{\left(E_x^{\mathrm{miss}}\right)^2 + \left(E_y^{\mathrm{miss}}\right)^2},$$

where the sum is over topological cluster cells within the pseudo-rapidity range $|\eta| < 4.5$. In the muon channel, the transverse momentum of the well-isolated muon selected in the analysis ($p_{\mathrm{T}} > 20$ GeV, see Section 6) is added – vectorially – to the (x,y) components of the missing transverse energy [3].

[3] Using the EM scale signals for all cells to reconstruct $E_{\mathrm{T}}^{\mathrm{miss}}$ does not yield an optimal measure for the real missing transverse energy, in particular in the presence of jets. A more refined measurement of $E_{\mathrm{T}}^{\mathrm{miss}}$, based on dedicated calibration factors for the various physics objects, is now available and will be used in the next stage of the analysis.

Missing Transverse Energy Significance (MetSig**)** is defined as the ratio of the $E_{\mathrm{T}}^{\mathrm{miss}}$ described above and the square root of the sum of the transverse energy deposited in the calorimeter cells at the electromagnetic energy scale. For the muon channel, the transverse momentum of the selected muons is consistently included in the MetSig calculation.

$$\mathrm{MetSig} \equiv E_{\mathrm{T}}^{\mathrm{miss}} / \sqrt{\sum E_T}$$

Effective Mass ($\mathrm{M_{eff}}$**)** is constructed from the highest p_{T} jets in the event (njet, up to a maximum of four jets), the $E_{\mathrm{T}}^{\mathrm{miss}}$ and the p_{T} of leptons (nlep) with $p_{\mathrm{T}} > 20$ GeV.

$$\mathrm{M_{eff}} \equiv E_{\mathrm{T}}^{\mathrm{miss}} + \sum_{i=1}^{\mathrm{njet}} |\mathbf{p}_{\mathrm{T}}^{(i)}| + \sum_{j=1}^{\mathrm{nlep}} |\mathbf{q}_{\mathrm{T}}^{(j)}|$$

Transverse Mass ($\mathrm{M_T}$**)** is used in the lepton channels and is constructed from the highest p_{T} lepton, with $p_{\mathrm{T}} >$20 GeV, and the $E_{\mathrm{T}}^{\mathrm{miss}}$ as follows:

$$\mathrm{M_T^2} \equiv 2|\mathbf{p}_{\mathrm{T}}^{\ell}||E_{\mathrm{T}}^{\mathrm{miss}}| - 2\mathbf{p}_{\mathrm{T}}^{\ell} \cdot \vec{E_{\mathrm{T}}^{\mathrm{miss}}}.$$

5.2 Overlap Removal

In the process of identifying physical objects, a classification is needed to resolve ambiguities. Based on previous studies [34], the criteria to remove the overlap use the radial distance ΔR and are applied in the following order:

1. If an electron and a jet are found within $\Delta R < 0.2$, the object is interpreted as an electron and the overlapping jet is ignored.
2. If a muon and a jet are found within $\Delta R < 0.4$, the object is treated as a jet and the muon is ignored.
3. If an electron and a jet are found within $0.2 < \Delta R < 0.4$, the object is interpreted as a jet and the nearby electron is ignored.

5.3 *b*-tagging

The identification of jets which originated from *b*-quarks (*b*-tagging) is based on the presence of a displaced vertex due to the decay of a *b* hadron inside the jet. The secondary vertex based SV0 tagger, whose performance on data has been reported in [29], is employed. SV0 is a lifetime-based *b*-tagger algorithm which explicitly reconstructs secondary vertices from tracks associated with a jet. The definition of an 'operating' point for the algorithm involves placing a threshold on the signed decay length significance of the reconstructed secondary vertex ($L/\sigma(L)$, where L is the decay length and $\sigma(L)$ the resolution). This quantity is sometimes referred to as "weight" (w). The sign of $L/\sigma(L)$ is given by the projection of the decay length on the jet axis. A list of tracks associated to the calorimeter jet is provided as input to the algorithm, which starts by reconstructing two-track vertices significantly displaced from the primary vertex in three dimensions. Input tracks are not allowed to be associated to multiple jets but only to the closest one ($\Delta R(\mathrm{jet} - \mathrm{track}) < 0.4$).

Candidate jets for *b*-tagging considered in this analysis are required to have $p_{\mathrm{T}} > 30$ GeV and $|\eta| < 2.5$. To achieve a good rejection against charm- and light-quark (u,d,s) or gluon-originated jets and, at the same time, keep a reasonable efficiency for *b*-quark jets, a signed

$L/\sigma(L)$ value greater than 6 has been chosen to identify b-jets. Based on Monte Carlo simulation studies of QCD multijet and top pair production samples, this value corresponds to an average b-tagging efficiency of 45-50%. Due to the dependence of the tagging algorithm on the p_{T} and η of the jet candidates, different average performances are expected for physical processes leading to different event topologies. Figure 2 shows the b-tagging efficiency and the tagging efficiency for u,d,s-quark or gluon jets (light-jet tagging efficiency) as a function of jets p_{T} and $|\eta|$ for QCD multijet and $t\bar{t}$ production processes. Efficiencies for SU4 signal samples are also shown for illustration. The b-tagging efficiency varies from 40% at low p_{T} to 65% at higher p_{T}, with a light-jet tagging efficiency at the level of $1\% - 2\%$.

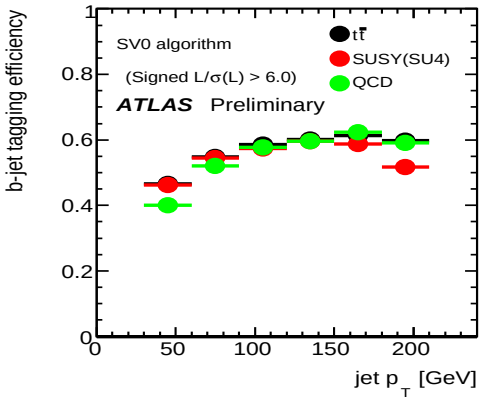

(a) b-tagging efficiency as a function of jet p_{T}.

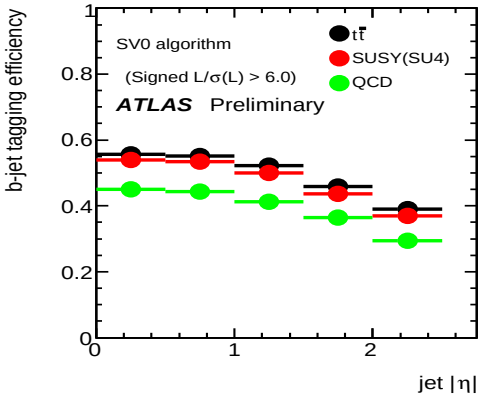

(b) b-tagging efficiency as a function of jet $|\eta|$.

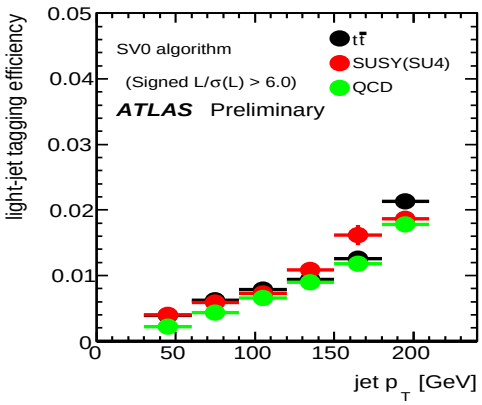

(c) Light-jet efficiency as a function of p_{T}

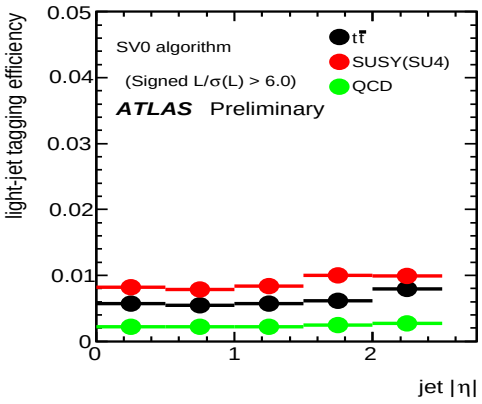

(d) Light-jet efficiency as a function of $|\eta|$

Figure 2: Monte Carlo efficiencies of b-tagging (*top*) and light-jet tagging (*bottom*) for $p_{\mathrm{T}} >$ 30 GeV jets, as obtained with SV0 tagger with threshold greater than 6, as a function of p_{T} (*left*) and $|\eta|$ (*right*) for $t\bar{t}$, SU4 and QCD multijet samples.

6 Event Selection

Typical event selection requirements for SUSY searches have been extensively discussed in previous studies [35] based on Monte Carlo simulations. For the purpose of this analysis, in which a first comparison of data to Monte Carlo is made for key observables, a looser set of selections, as defined in Table 2, is employed. Pre-selection requirements are similar for no

lepton, electron and muon final states and include: rejection of events with misidentified jets ('clean up cuts'); rejection of events with reconstructed electrons pointing to the calorimeter barrel–endcap transition region $1.37 < |\eta| < 1.52$ ('electron fiducial cut'); and rejection of events with no primary reconstructed vertex with at least five associated tracks. The selections specific to the different channels are reported in the following.

0-lepton	Electron	Muon
Pre-selection cuts: data quality, trigger requirements; clean up for misidentified jets; electron fiduciality; $\geq$1 primary vertex with $\geq$5 tracks		
No lepton ($p_{\mathrm{T}} > 10$ GeV)	≥ 1 electron ($p_{\mathrm{T}} > 20$ GeV)	≥ 1 muon ($p_{\mathrm{T}} > 20$ GeV)
2-jet: jet $p_{\mathrm{T}} > (70, 30)$ GeV 3-jet: 3rd jet $p_{\mathrm{T}} > 30$ GeV	jet $p_{\mathrm{T}} > (30, 30)$ GeV -	jet $p_{\mathrm{T}} > (30, 30)$ GeV -
$E_{\mathrm{T}}^{\mathrm{miss}} / \sqrt{\sum E_T} > 2$ GeV$^{1/2}$		
At least 1 b-tagged jet ($L/\sigma(L) > 6$, $p_{\mathrm{T}} > 30$ GeV)		

Table 2: Event selection for the different final states considered: 0-lepton (2- and 3-jet selections), ≥ 1 electron and ≥ 1 muon.

Final states with no leptons (0-lepton channel) Events are selected to have a leading jet of $p_{\mathrm{T}} > 70$ GeV in order to reduce uncertainties due to trigger threshold effects, and at least one additional jet with $p_{\mathrm{T}} > 30$ GeV. All jets are required to have $|\eta| < 2.5$. In order to define exclusive channels, events with electrons (muons) with $p_{\mathrm{T}} > 10$ GeV and $|\eta| < 2.47$ ($|\eta| < 2.4$) are rejected. For the 3-jet topology, the p_{T} of the third leading jet is required to be above 30 GeV. The sample of interest ('signal' region) is defined by selecting events with MetSig > 2 GeV$^{1/2}$, implemented to reject part of the Standard Model background. An event selection based on MetSig rather than on $E_{\mathrm{T}}^{\mathrm{miss}}$ reduces the dependence on the energy scale. At the moment, this choice is preferred since $E_{\mathrm{T}}^{\mathrm{miss}}$ is calibrated at EM scale whilst the jets are corrected to the hadronic energy scale. The correlation between the MetSig and $E_{\mathrm{T}}^{\mathrm{miss}}$ is such that a threshold on MetSig of 2 GeV$^{1/2}$ approximately corresponds to a cut on $E_{\mathrm{T}}^{\mathrm{miss}}$ of about 30 GeV.

The low MetSig region is considered as 'control' sample and used to estimate the normalization of the QCD multijet predictions from Monte Carlo simulation, as described in Section 7.2. Finally, at least one b-tagged jet, defined as in Section 5.3, is required among all jets with p_{T} above 30 GeV.

Final states with at least one lepton (electron/muon channel) These events are defined by the presence of at least one electron (muon) with $p_{\mathrm{T}} > 20$ GeV. Electron candidates are required to have $|\eta| < 2.47$, muon candidates to have $|\eta| < 2.4$. In both cases, the transverse momentum cuts are chosen to minimize possible trigger threshold effects. In addition, two jets of $p_{\mathrm{T}} > 30$ GeV and MetSig > 2 GeV$^{1/2}$ are required, together with the presence of at least 1 b-tagged jet. If the event includes a muon with $p_{\mathrm{T}} > 20$ GeV, the transverse momentum is added to the $E_{\mathrm{T}}^{\mathrm{miss}}$ and MetSig calculations, as described in Section 5.1.

7 Normalization of QCD Background

QCD multijet processes constitute the dominant background for this analysis. These processes are estimated with the PYTHIA QCD Monte Carlo, which is only leading order in the strong coupling constant and therefore not expected to correctly describe the absolute normalization of the QCD cross section. Thus, dedicated control regions are defined for each of the channels to determine the QCD normalization from data.

7.1 No-Lepton Final States

The control region for the 0-lepton channel is identified by requiring all the events to pass the dijet selection and to have MetSig <2 $\text{GeV}^{1/2}$. This region is dominated by QCD multijet production and negligible contributions from other processes such as top and W/Z bosons plus jets production are expected. The ratio between data and QCD Monte Carlo estimation is found to be 0.61, with negligible statistical uncertainties. Figure 3 shows the MetSig distribution for events with two jets of $p_{\text{T}} > 70$ GeV and $p_{\text{T}} > 30$ GeV after the preselection cuts, once the normalization factor is applied. Good agreement between data and Standard Model expectation is found over the entire range. The band includes the statistical and systematic uncertainties.The data/QCD Monte Carlo ratio can be determined before and after requiring at least one *b*-tagged jet in the events. The normalization values obtained with the two samples – in the following, referred to as "inclusive" and "*b*-tag", respectively – are compared and the difference is accounted for as a systematic uncertainty. Such differences might arise from discrepancies in terms of *b*-tagging performance between data and Monte Carlo and from an imperfect modelling of heavy-flavour production in the QCD multijet Monte Carlo simulation (see Section 8). Table 3 summarizes the number of events from the data and the PYTHIA QCD Monte Carlo prediction before and after requiring at least 1 *b*-tag jet with p_{T} above 30 GeV and $|\eta|$ <2.5.

Selection	data	QCD	data/QCD
MetSig < 2 $\text{GeV}^{1/2}$ (inclusive)	463180	752913	0.61
MetSig < 2 $\text{GeV}^{1/2}$ (≥ 1 *b*-tag jet)	28638	42562	0.67

Table 3: Number of events observed in the data and the PYTHIA prediction in QCD-dominated control samples.

7.2 One-Lepton Final States

The strategy used to obtain the absolute normalization of the QCD multijet PYTHIA sample to data is similar to the procedure applied for the 0-lepton channel. However, in this case the presence of electroweak and top production contributions is non-negligible. Thus, the control region has been defined to be orthogonal to the signal regions by reversing the MetSig requirement, and applying an extra cut on the transverse mass, M_{T}, between the lepton and the $E_{\text{T}}^{\text{miss}}$.The resulting control sample contains events with at least one lepton, 2 jets with $p_{\text{T}} > 30$ GeV, $\text{M}_{\text{T}} < 40$ GeV and MetSig < 2 $\text{GeV}^{1/2}$. The selected samples in the electron and muon case are expected to be dominated by QCD multijet production. The remaining non-QCD background contributions estimated from Monte Carlo are of the order of a few percent and are subtracted from the number of data events when normalizing the QCD sample. The normalization factors obtained in this way are shown in Table 4. Since the normalization is meant to

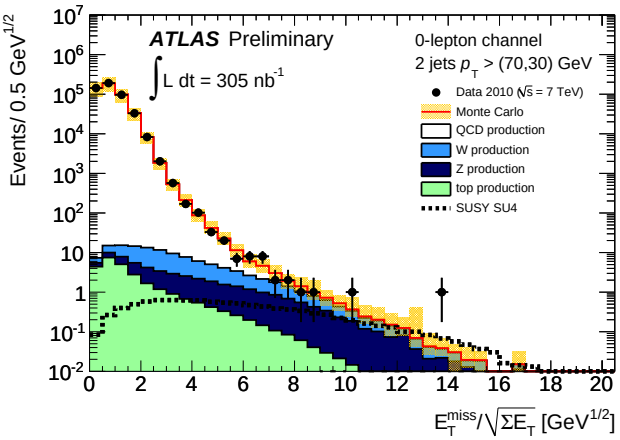

Figure 3: Missing Transverse Energy Significance (MetSig) distribution for events passing dijet selection. The data are compared to Standard Model expectations obtained from Monte Carlo samples after applying the normalization factor for the QCD background. No b-tagging requirement is implemented at this stage. The yellow band indicates the total systematic uncertainty (see Section 8). For illustration, the SU4 supersymmetry benchmark point is also shown: negligible contribution in the control region is expected.

Selection	data	QCD	non-QCD	(data – non-QCD) /QCD
Electron channel	353	1070±170	7.23±0.07	0.32 ±0.05
Electron channel after b-tagging	15	70±20	0.65±0.01	0.21 ± 0.08
Muon channel	70	143±5	5.07±0.06	0.45±0.05
Muon channel after b-tagging	9	29±2	0.55±0.01	0.30± 0.10

Table 4: Number of events in data and Monte Carlo predictions for the control region used to normalize the QCD multijet background. The control region is defined by $M_{\mathrm{T}} < 40$ GeV and MetSig <2 GeV$^{1/2}$. Results are also given with the extra requirement of at least one b-tagged jet with $p_{\mathrm{T}} > 30$ GeV and $|\eta| < 2.5$. The normalization factors are calculated after subtracting from the data the non-QCD background predicted by the Monte Carlo.

include possible effects due to electron and muon misidentification, the factors are derived separately for each lepton species, and are different from those obtained in the 0-lepton channel. In the case of the muon channel, the QCD muon-filtered Monte Carlo samples, described in Section 4, have been considered. Normalization values have been also compared after the requirement of at least one b-tagged jet with $p_{\mathrm{T}} > 30$ GeV and $|\eta| < 2.5$. In this case, the statistical fluctuations are higher and the resulting factors for the two samples are compatible.

Figure 4 shows the transverse mass for electron and muon final states in the control samples defined by MetSig <2 GeV$^{1/2}$ and after the corresponding QCD Monte Carlo normalization factors from inclusive control regions have been applied. Agreement between data and Standard Model expectation is observed in the entire range.

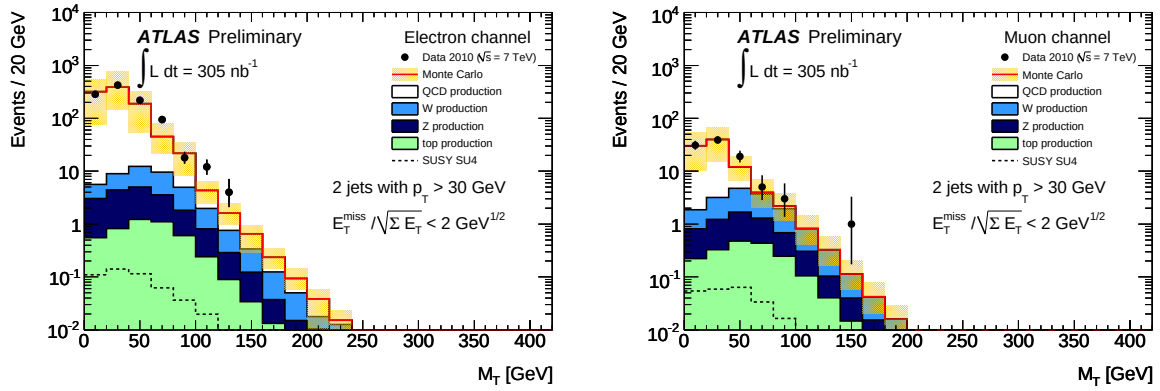

Figure 4: M_T distribution for events in electron (*left*) and muon (*right*) samples, for MetSig <2 GeV$^{1/2}$. The data are compared to Standard Model expectations obtained from Monte Carlo samples after applying the normalization factors for the QCD background. No *b*-tagging requirement is implemented at this stage. The yellow band indicates the total systematic uncertainty (see Section 8). For illustration, the SU4 supersymmetry benchmark point is also shown: negligible contribution in the control regions is expected.

8 Systematic Uncertainties

Several sources of systematic uncertainties on the Standard Model prediction have been studied, and are added in quadrature for the estimation of the total uncertainty.

Jet Energy Scale The uncertainty associated with the jet energy scale has been estimated using a parametrization of this scale as a function of jet p_T and η [31]. The jet energy scale uncertainties vary between 10% for jets in the range 20 GeV $< p_T <$ 60 GeV and 7% for jets at higher p_T. The effects of energy scale changes have been determined by rescaling jet energies and momenta in all Monte Carlo simulated samples. A coherent recalculation of the E_T^{miss} with the rescaled energies of the clusters associated with the jets is also performed.

The resulting systematic uncertainty on the number of expected events from Standard Model processes is approximately 30% for both 0-lepton and 1-lepton channels after all selections. However, the current estimate of the jet energy scale uncertainty is conservative, and will soon be reduced by using $in-situ$ methods. An additional uncertainty of about 1% is considered to account for the uncertainties due to extra proton-proton interactions in the same bunch crossing (in-time pile-up). No specific corrections or additional uncertainties on the *b*-jets energy scale are applied at this stage, since the effects are expected to be small compared to the jet energy scale uncertainties.

Unclustered energy A 20% fully correlated uncertainty is applied to take into account the MetSig sensitivity to the underlying event and to the energy of calorimeter cells not contained within the jets. The uncertainty is estimated in the large statistics 0-lepton channel sample, comparing the predictions of the nominal QCD multijet Monte Carlo with those obtained with a `PYTHIA` sample with increased activity from multiple parton interactions (ATLAS MC08 tuning, see [17]). The 20% uncertainty is applied to the 0- and 1-lepton channels.

Tagging performance The differences between the tagging algorithm performance in data and in Monte Carlo simulation are taken as systematic uncertainties, using the large statistics of "inclusive" and "*b*-tag" control samples for the 0-lepton channel (see Section 7.2). These differences are quantified using the signed $L/\sigma(L)$ distribution. Figure 5 shows the distribution of $L/\sigma(L)$ for all jets with $p_{\mathrm{T}} > 30$ GeV after the inclusive dijets selection for data and Monte Carlo in the low MetSig control sample and after applying the global normalization factor 0.61. For illustration, the *b*-jet content of the QCD multijet Monte Carlo is also reported. Deviations of $\sim 30\%$ are observed in the negative $L/\sigma(L)$ region, which is mostly dominated by light-quark jets. However, in the positive $L/\sigma(L)$ region this effect is mitigated by the larger presence of real *b*-jets. Thus, deviations from unity for the ratio between data and Monte Carlo are estimated in the region with $L/\sigma(L) > 6$ (*b*-tag candidates) and are found to be of the order of 10%.

This estimation of the uncertainties does not take into account possible differences between control and signal regions in terms of real *b*-jet content and in terms of light-jets tagging efficiency. The latter is estimated as the fraction of events with at least one jet with negative signed $L/\sigma(L)$. Such fraction is found to be larger in the signal region with respect to the control region by a factor 1.16. This value is smaller than the difference between the real *b*-jet content in the control and in the signal regions, which is found to be a factor of 2. Thus, assuming that the uncertainty on the deviation between data and Monte Carlo is driven by the efficiency of tagging real *b*-jets, the 10% uncertainty has been conservatively enlarged by this factor, providing an overall 20% uncertainty on the tagging performance.

Further checks in the control sample show that the QCD Monte Carlo prediction is in general agreement with data for the kinematic range explored in this analysis within uncertainty. As an example, Figure 6 shows the inclusive jet p_{T} distribution in data and QCD Monte Carlo before and after *b*-tagging requirements, for events in the control sample after applying the normalization factor, as well as their ratios. At high p_{T} (>200 GeV) the jet spectrum shows a slight underestimation of PYTHIA predictions with respect to data, as expected from a LO Monte Carlo. The double ratio shows that differences in tagging performance in data and simulated events are within 20% uncertainty.

The 20% uncertainty is consistently applied to all the Standard Model Monte Carlo contributions in the 0- and the 1-lepton channels.

Normalization of the QCD background For the 0-lepton channel, the uncertainty on tagging performance is dominant, therefore no additional uncertainties have been applied. For the 1-lepton channels, a total uncertainty of 50% is applied to the QCD normalization factors, to take into account also possible differences between data and Monte Carlo in terms of lepton identification efficiency [10].

Luminosity As the QCD multijet Monte Carlo predictions are normalized to data, there is no need to apply any luminosity systematics to this contribution. For all other backgrounds a luminosity uncertainty of $\pm 11\%$ is assigned.

Non-QCD backgrounds The uncertainties on the normalization of associated production of W/Z boson and jets and top production backgrounds will be determined with data-driven techniques when more data are acquired. At this stage, a conservative uncertainty of 60% is assumed for associated production of boson and jets, to take into account uncertainties on the predicted cross sections, on the modeling of the initial- and final-state soft gluon radiation, and on the PDFs. No additional systematics are assigned to the top production, since they are neg-

ligible compared to the jet energy scale, tagging and luminosity uncertainties.

PYTHIA Monte Carlo predictions for QCD multijet processes have been compared to those from ALPGEN samples. Differences in shape for distributions measured in this analysis have been found to be small compared to the total experimental uncertainties. Thus, no attempt has been made to assign uncertainties on the normalization factor related to the predictions of different QCD Monte Carlo generators.

The resulting relative systematic uncertainties on the Standard Model expectations after applying all selections are collected in Table 5 for the 0-lepton and 1-lepton channels.

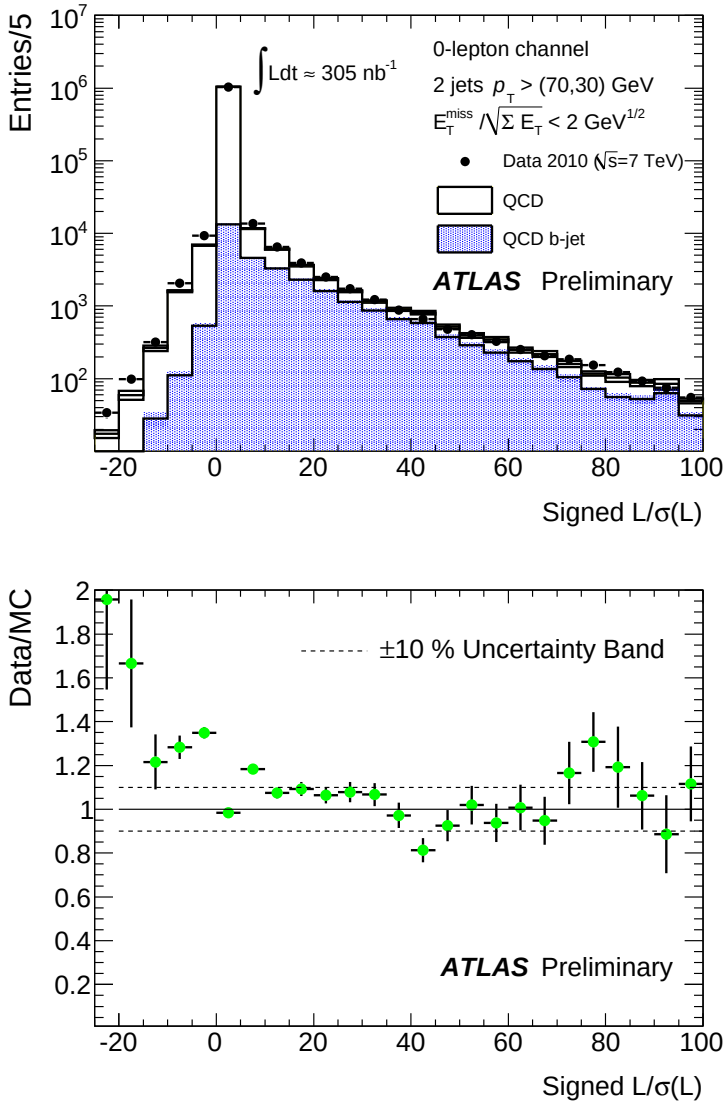

Figure 5: Signed decay length significance $L/\sigma(L)$ of the reconstructed secondary vertex for all jets in events passing the dijet event selection cuts and MetSig < 2 GeV$^{1/2}$, for data and Monte Carlo (MC) expectations. The ratio data/MC is also shown on the bottom.

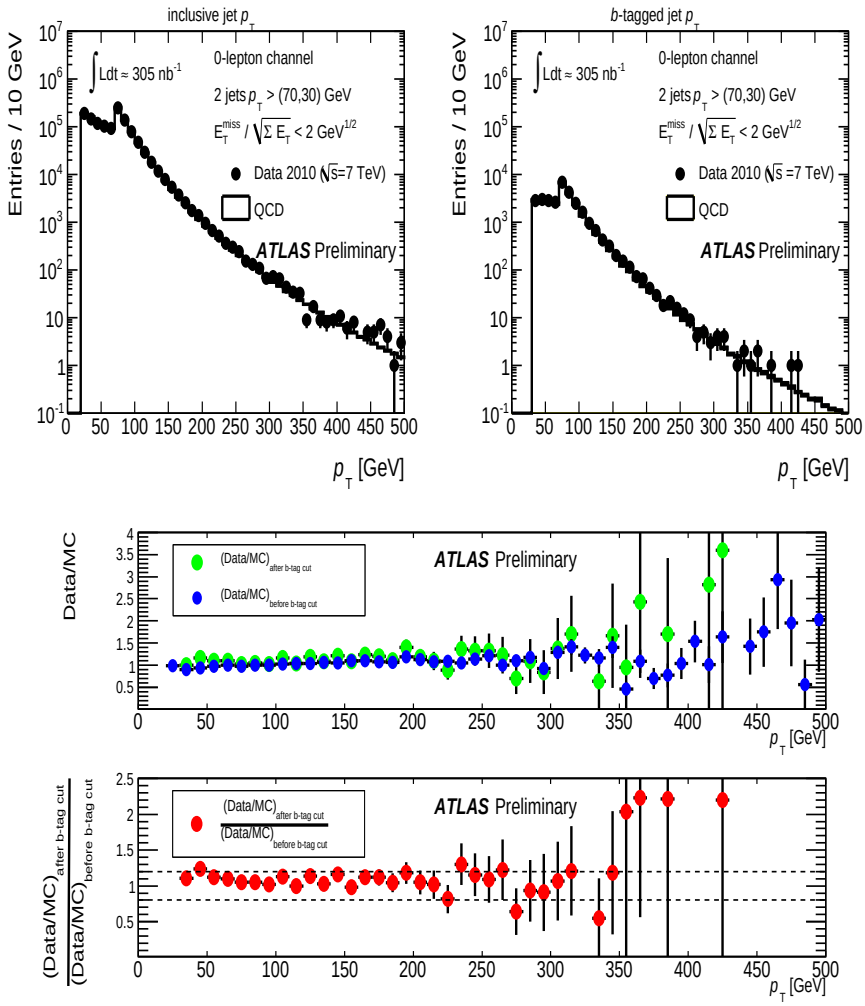

Figure 6: Inclusive jet p_{T} distribution (*left*) and b-tagged jet p_{T} distribution (*right*) for events in the low MetSig 0-lepton control sample. The middle plot shows the ratio between data and QCD dijet Monte Carlo (MC) expectations and the bottom plot shows the double ratio. The dashed band indicates the final 20% systematic uncertainty assigned to tagging performance.

Source of uncertainty	0-lepton	1-lepton
Jet Energy Scale (including pile-up)	$\sim \pm$ 30%	$\sim \pm$25%
Unclustered Energy	$\pm$20%	$\pm$20%
Tagging Performance	$\pm$20%	$\pm$20%
Lepton Identification Performance	–	$\pm$50%
Luminosity	$\pm$11%	$\pm$11%
Theory	$\pm$60%	$\pm$60%

Table 5: Relative systematic uncertainties on the Standard Model expected number of events after all selections are applied for the 0-lepton and 1-lepton channels. Uncertainties on lepton identification performance are applied to QCD background only via normalization factors. Uncertainties on the luminosity are applied on non-QCD backgrounds only. Uncertainties on the theory refer to W/Z boson plus jets production as explained in the text.

9 Results and Distributions for the 0-Lepton Channel

In this section, events observed in data are compared to the number of events expected from Standard Model and SU4 SUSY processes as estimated in Monte Carlo simulation, for the 0-lepton selection. Distributions of most relevant quantities are shown after the final event selection is applied, for 2-jet and 3-jet topologies.

9.1 2-jet Selection

The number of events in the data and the overall expectation from Standard Model processes are shown in Table 6 after each event selection step for the dijet selection of the 0-lepton channel. The corresponding expectations from the supersymmetry scenario chosen as reference are also given. The statistical and systematic uncertainties described in Section 8 are added in quadrature. Systematic uncertainties might be asymmetric due to the propagation of the jet energy scale uncertainties. The percentage of reconstructed events that fulfill the *b*-tagging requirements after the MetSig > 2 GeV$^{1/2}$ cut is 12%. The percentage of the Monte Carlo events with a *b*-tagged jet matched to a true *b*-quark [4] is 75%.

The breakdown of the different Standard Model contributions is presented in Table 7. As expected because of the relatively low $E_{\mathrm{T}}^{\mathrm{miss}}$ selection ($\simeq$ 30 GeV), QCD multijet production processes dominate 0-lepton final states.

2-jet selection	data	Standard Model expectation	SU4
Jets $p_{\mathrm{T}} > (70, 30)$ GeV	474243	$(4.7^{+2.1}_{-1.9}) \cdot 10^5$	9.95±0.06
MetSig > 2 GeV$^{1/2}$	11190	$(1.1^{+0.5}_{-0.6}) \cdot 10^4$	8.71±0.06
At least 1 *b*-tagged jet	1253	1190 ± 430	4.23±0.04

Table 6: Number of events observed in the data and expected contributions of the different Standard Model processes for the 2-jet 0-lepton event selection. The expectations for the reference SU4 supersymmetry scenario are also given. The quoted uncertainties include statistical and systematic contributions, except for the SU4 results, for which only the statistical uncertainties are given.

2-jet selection	QCD	*W*+jets	*Z*+jets	top
Jets $p_{\mathrm{T}} > (70, 30)$ GeV	$(4.72 \pm 0.01) \cdot 10^5$	71.1 ± 0.3	28.6 ± 0.2	26.4 ± 0.07
MetSig > 2 GeV$^{1/2}$	$(1.11 \pm 0.02) \cdot 10^4$	47.4 ± 0.2	19.3 ± 0.2	6.73 ± 0.02
At least 1 *b*-tagged jet	1181 ± 36	2.18 ± 0.04	0.74 ± 0.03	4.51 ± 0.02

Table 7: Breakdown of the different processes contributing to the Standard Model expectation for the 2-jet 0-lepton event selection. Only statistical uncertainties are given.

Relevant *b*-tagging-related quantities, such as the SV0 $L/\sigma(L)$, the *b*-tagged jet multiplicity and the p_{T} of the highest SV0 $L/\sigma(L) > 6$ *b*-tagged jet are shown in Figure 7 for data, the main Standard Model contributions and the SU4 reference supersymmetry scenario. Generally, good agreement is found between data and Standard Model expectations estimated from Monte Carlo, for all these quantities. At high p_{T} (>200 GeV), the *b*-tagged jet spectrum shows

[4] In Monte Carlo simulated events, a jet is labelled as true *b*-jet if a *b*-quark is found at maximum distance $\Delta R = 0.3$ with respect to the jet axis.

that the PYTHIA QCD multijet prediction slightly underestimates the data, as it is expected for a $2 \rightarrow 2$ LO generator [36].

Data and Monte Carlo expectations are also in good agreement for complex variables like $E_{\mathrm{T}}^{\mathrm{miss}}$ significance and effective mass $\mathrm{M_{eff}}$, as shown in Figure 8. Figure 9 shows other key observables for SUSY searches such as the azimuthal distance between the *b*-tagged jet with the highest SV0 $L/\sigma(L)$ and the $E_{\mathrm{T}}^{\mathrm{miss}}$ direction, and the $E_{\mathrm{T}}^{\mathrm{miss}}/\mathrm{M_{eff}}$ fraction.

QCD multijet background with large $E_{\mathrm{T}}^{\mathrm{miss}}$ originates from misreconstruction of the jet energies in the calorimeters. In such events the $E_{\mathrm{T}}^{\mathrm{miss}}$ direction tends to be aligned, in the transverse plane, with one of the leading jets in the event. Previous studies [35] based on Monte Carlo simulations have shown that high suppression of QCD multijet background is achieved by requiring a minimum azimuthal distance between the leading jets and the $E_{\mathrm{T}}^{\mathrm{miss}}$ direction, $\Delta\phi_{\mathrm{min}}(E_{\mathrm{T}}^{\mathrm{miss}},\mathrm{jet})$. Figure 10 shows the $\Delta\phi_{\mathrm{min}}(E_{\mathrm{T}}^{\mathrm{miss}},\mathrm{jet})$ distribution, where the first three leading jets with p_{T} >20 GeV are considered, and the $\mathrm{M_{eff}}$ distribution for events passing the requirement $\Delta\phi_{\mathrm{min}}(E_{\mathrm{T}}^{\mathrm{miss}},\mathrm{jet}) > 0.2$: 446 events are found in data, in good agreement with the expectation of 410^{+150}_{-180}. About 65% of the events are rejected by this selection.

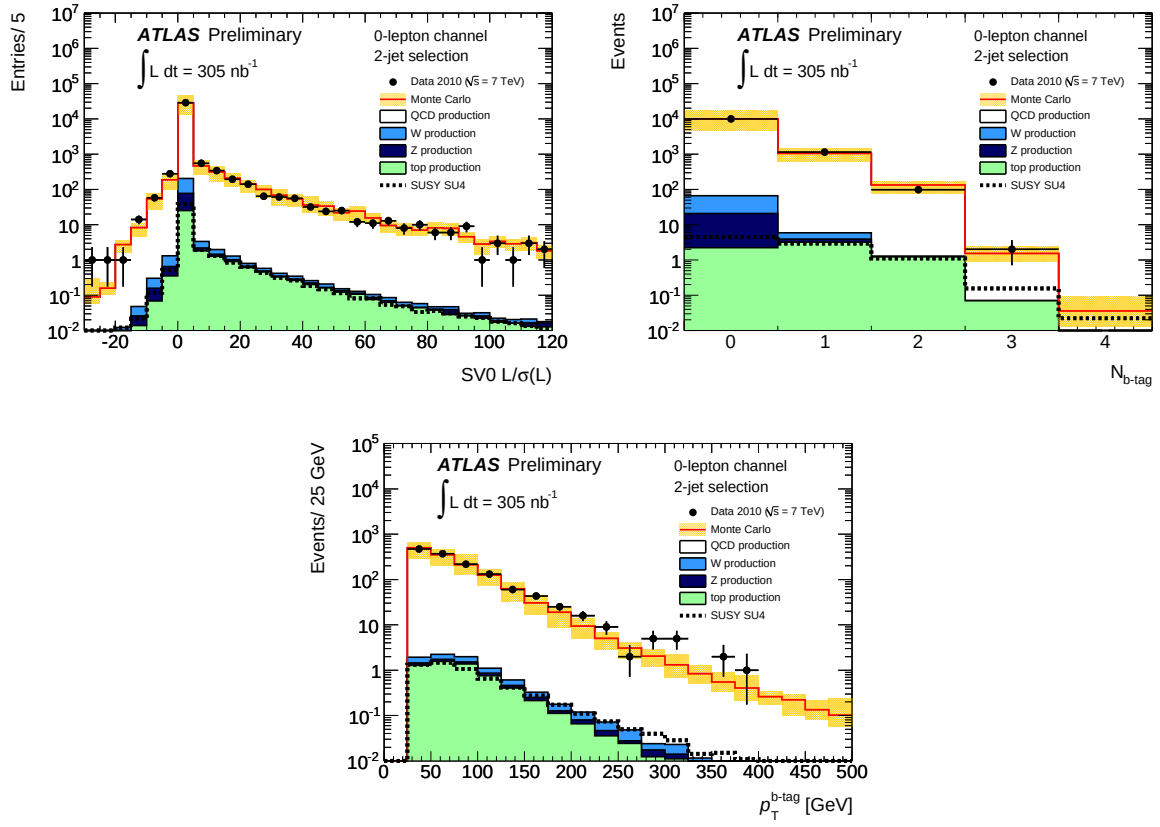

Figure 7: *b*-tag SV0 $L/\sigma(L)$ distribution (*left*), multiplicity of *b*-tagged jets (*right*) and p_{T} distribution for the highest SV0 $L/\sigma(L) > 6$ *b*-tagged jet (*bottom*) for data and the different Standard Model contributions before the *b*-tagged jet requirement for the 0-lepton 2-jet event selection. The uncertainty band includes statistical and systematic uncertainties. The SU4 supersymmetry benchmark point is also shown.

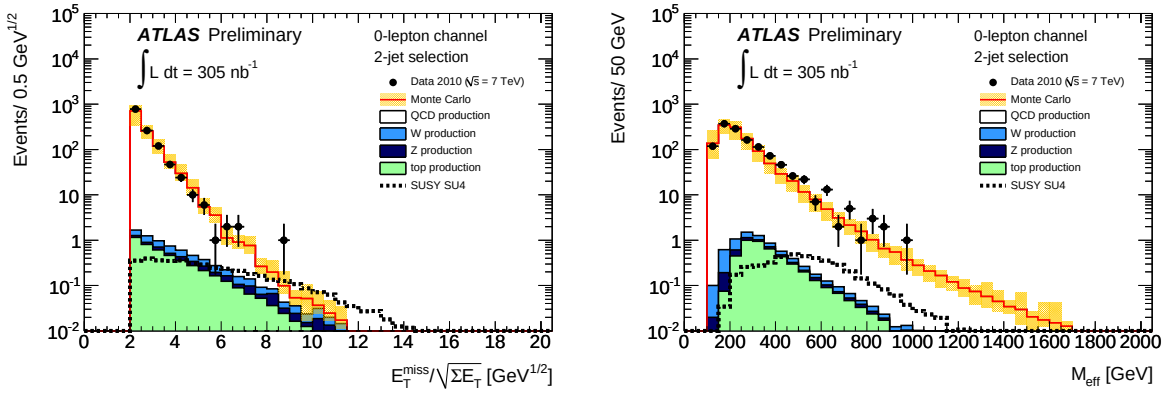

Figure 8: MetSig (*left*) and Effective Mass M_{eff} (*right*) for data and the different Standard Model contributions after the 0-lepton 2-jet event selection is applied. The uncertainty band includes statistical and systematic uncertainties. The SU4 supersymmetry benchmark point is also shown.

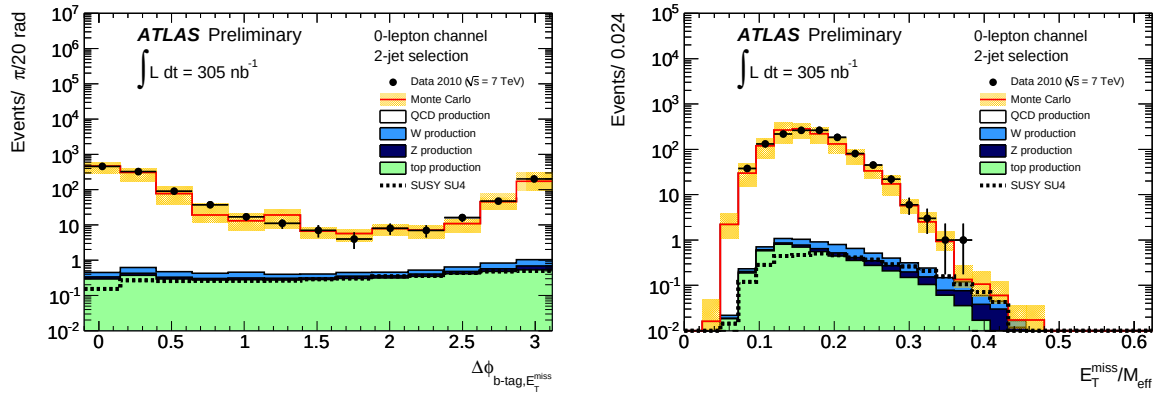

Figure 9: Azimuthal angle between the *b*-tagged jet with highest SV0 $L/\sigma(L)$ and the $E_{\mathrm{T}}^{\mathrm{miss}}$ vector (*left*) and the $E_{\mathrm{T}}^{\mathrm{miss}}/\mathrm{M_{eff}}$ ratio (*right*) for data and the different Standard Model contributions after the 0-lepton 2-jet event selection is applied. The uncertainty band includes statistical and systematic uncertainties. The SU4 supersymmetry benchmark point is also shown.

9.2 3-jet Selection

After the 3-jet selection is applied, 429 data events remain, in agreement with the Standard Model Monte Carlo expectation of 400^{+160}_{-160}. The number of events for supersymmetry bench mark point SU4 is approximately the same as in the 2-jet selection. The MetSig, the M_{eff} and the p_{T} of the leading jet and the highest *b*-tagged SV0 $L/\sigma(L)$ jet after the 3-jet event selection is applied are shown in Figure 11. Good agreement between data and Standard Model expectations is observed within the statistical and systematic uncertainties in all regions of phase space covered with the current dataset.

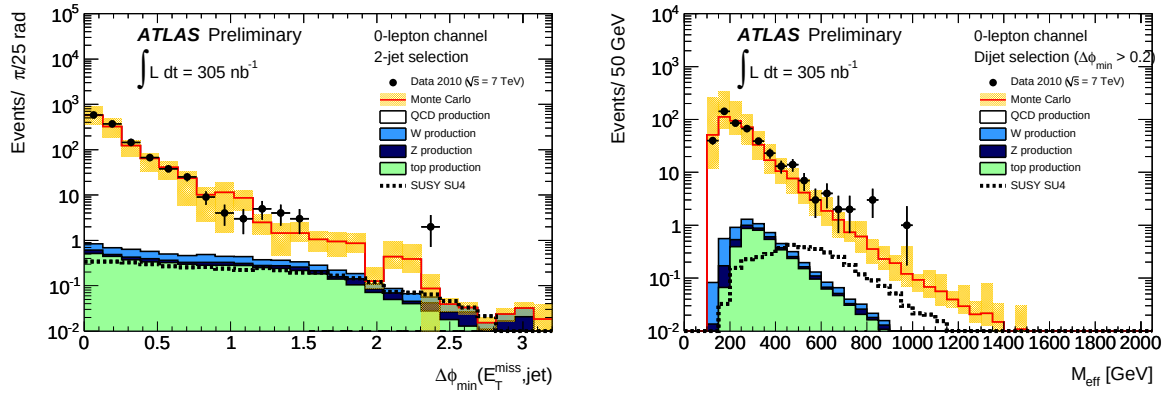

Figure 10: Minimal azimuthal angle between the jets with highest p_{T} and the $E_{\mathrm{T}}^{\mathrm{miss}}$ (*left*) and the Effective mass ($\mathrm{M_{eff}}$) distribution after $\Delta\phi_{\mathrm{min}}(E_{\mathrm{T}}^{\mathrm{miss}},\mathrm{jet}) > 0.2$ (*right*) for data and the different Standard Model contributions after the 0-lepton 2-jet event selection is applied. The uncertainty band includes statistical and systematic uncertainties. The SU4 supersymmetry benchmark point is also shown.

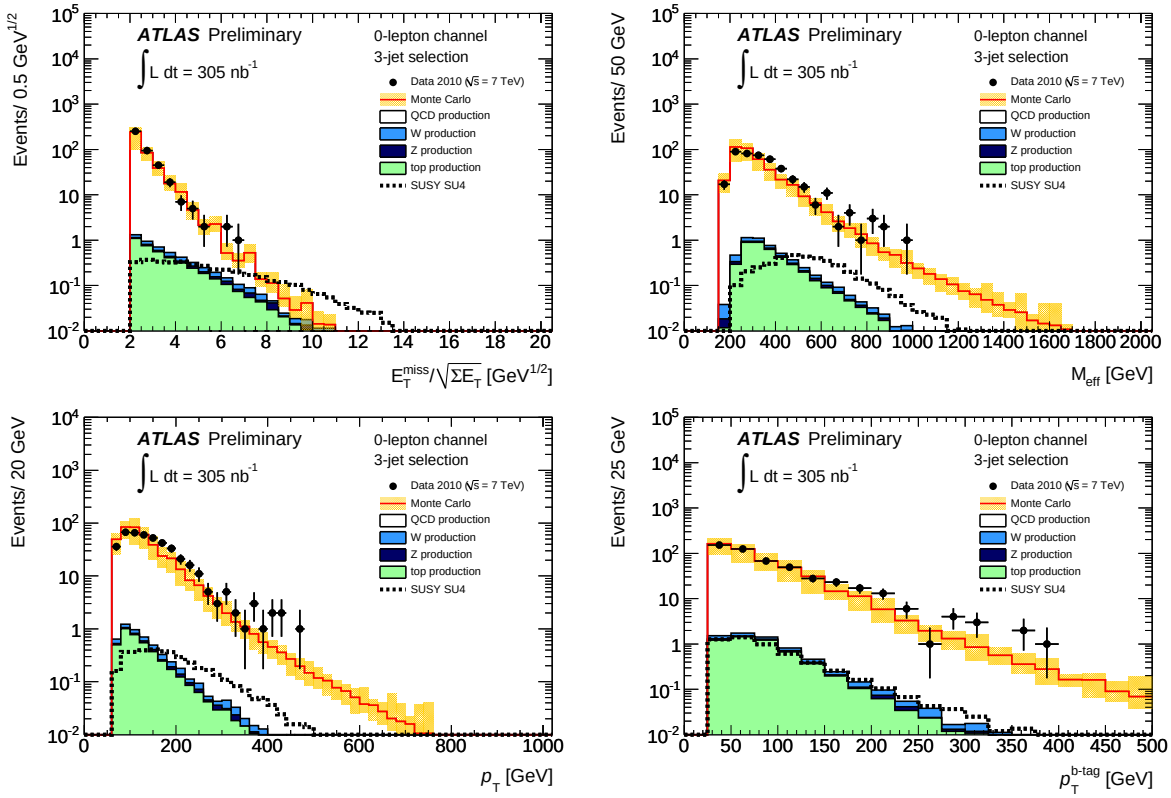

Figure 11: MetSig (*top left*), $\mathrm{M_{eff}}$ (*top right*), p_{T} of the leading jet (*bottom left*) and p_{T} of the highest SV0 $L/\sigma(L)$ b-tagged jet (*bottom right*) distributions for data and the different Standard Model contributions after the 0-lepton 3-jet event selection is applied. The uncertainty band includes statistical and systematic uncertainties. The SU4 supersymmetry benchmark point is also shown.

10 Results and Distributions for the 1-Lepton Channel

The number of events in the data and the overall expectation from Standard Model processes are shown in Table 8 – after each event selection step – for the electron channel, in which at least one electron of $p_{\mathrm{T}} > 20$ GeV is required. The corresponding expectations from the supersymmetry scenario chosen as reference are also given. The statistical and systematic uncertainties described in Section 8 are added in quadrature. Table 9 provides the breakdown of the main Standard Model contributions with their statistical uncertainties. QCD multijet processes still dominate after the requirement of at least one electron and two jets of $p_{\mathrm{T}} > 30$ GeV. However, after the MetSig > 2 GeV$^{1/2}$ cut, the dominant background process is the associated production of W boson and jets. After the requirement of at least one b-tagged jet, the dominant process is top production, followed by W+jet and QCD multijet processes. Analogous results for the muon channel, in which at least one muon of $p_{\mathrm{T}} > 20$ GeV is required, are shown in Table 10 and Table 11. The total Standard Model expectations are similar to those obtained for the electron channel, although the QCD multijet contribution is less significant.

After all selections are applied, 4 events remain for the electron channel, with a Standard Model expectation of $4.8^{+1.7}_{-1.5}$, and 8 events remain for the muon channel, with a Standard Model expectation of $4.7^{+1.7}_{-1.5}$. In both cases, data are in agreement with the Monte Carlo simulation, within statistical and systematic uncertainties. Since the electron and muon channels are not mutually exclusive, it has been verified that none of the data events pass both selections.

Electron channel	data	Standard Model	SU4
≥ 1 electron and 2 jets $p_{\mathrm{T}} > (30, 30)$ GeV	557	520^{+360}_{-330}	1.65 ± 0.02
MetSig > 2 GeV$^{1/2}$	31	39^{+28}_{-20}	1.40 ± 0.02
At least 1 b-tagged jet	4	$4.8^{+1.7}_{-1.5}$	0.81 ± 0.02

Table 8: Number of events observed in the data and expected contributions of the different Standard Model processes for the electron event selection. The expectations for the reference SU4 supersymmetry scenario are also given. The quoted uncertainties include statistical and systematic contributions, except for the SU4 results, for which only the statistical uncertainties are given.

Electron channel	QCD	W+jets	Z+jets	top
≥ 1 electron and 2 jets $p_{\mathrm{T}} > (30, 30)$ GeV	470 ± 57	38.3 ± 0.2	8.42 ± 0.08	7.22 ± 0.02
MetSig > 2 GeV$^{1/2}$	8.0 ± 1.0	25.4 ± 0.1	1.20 ± 0.03	4.67 ± 0.01
At least 1 b-tagged jet	0.78 ± 0.31	1.00 ± 0.03	0.10 ± 0.01	2.95 ± 0.01

Table 9: Breakdown of the different processes contributing to the Standard Model expectation in the electron channel. Only statistical uncertainties are given.

Figures 12 and 13 show the p_{T} of the leading jet, the p_{T} of the b-tagged jet with the highest SV0 $L/\sigma(L)$, the $\mathrm{M_{eff}}$ and the transverse mass between the lepton and the $E_{\mathrm{T}}^{\mathrm{miss}}$ for the data, the main Standard Model contributions and the SU4 reference supersymmetry scenario after all electron and muon channel event selections, respectively. The uncertainty band includes the statistical and systematic uncertainties assigned to the Monte Carlo expectations summed in quadrature.

Muon channel	data	Standard Model	SU4
≥ 1 muon and 2 jets $p_{\mathrm{T}} > (30, 30)$ GeV	138	130^{+70}_{-60}	1.58 ± 0.02
MetSig > 2 GeV$^{1/2}$	40	37^{+28}_{-19}	1.34 ± 0.02
At least 1 b-tagged jet	8	$4.7^{+1.7}_{-1.5}$	0.80 ± 0.02

Table 10: Number of events observed in the data and expected contributions of the different Standard Model processes for the muon event selection. The expectations for the reference SU4 supersymmetry scenario are also given. The quoted uncertainties include statistical and systematic contributions, except for the SU4 results, for which only the statistical uncertainties are given.

Muon channel	QCD	W+jets	Z+jets	top
≥ 1 muon and 2 jets $p_{\mathrm{T}} > (30, 30)$ GeV	74.4 ± 2.3	38.5 ± 0.2	7.14 ± 0.07	6.77 ± 0.02
MetSig > 2 GeV$^{1/2}$	1.7 ± 0.3	27.9 ± 0.1	2.83 ± 0.05	4.60 ± 0.01
At least 1 b-tagged jet	0.49 ± 0.14	1.09 ± 0.03	0.20 ± 0.01	2.93 ± 0.01

Table 11: Breakdown of the different processes contributing to the Standard Model expectation in the muon channel. Only statistical uncertainties are given.

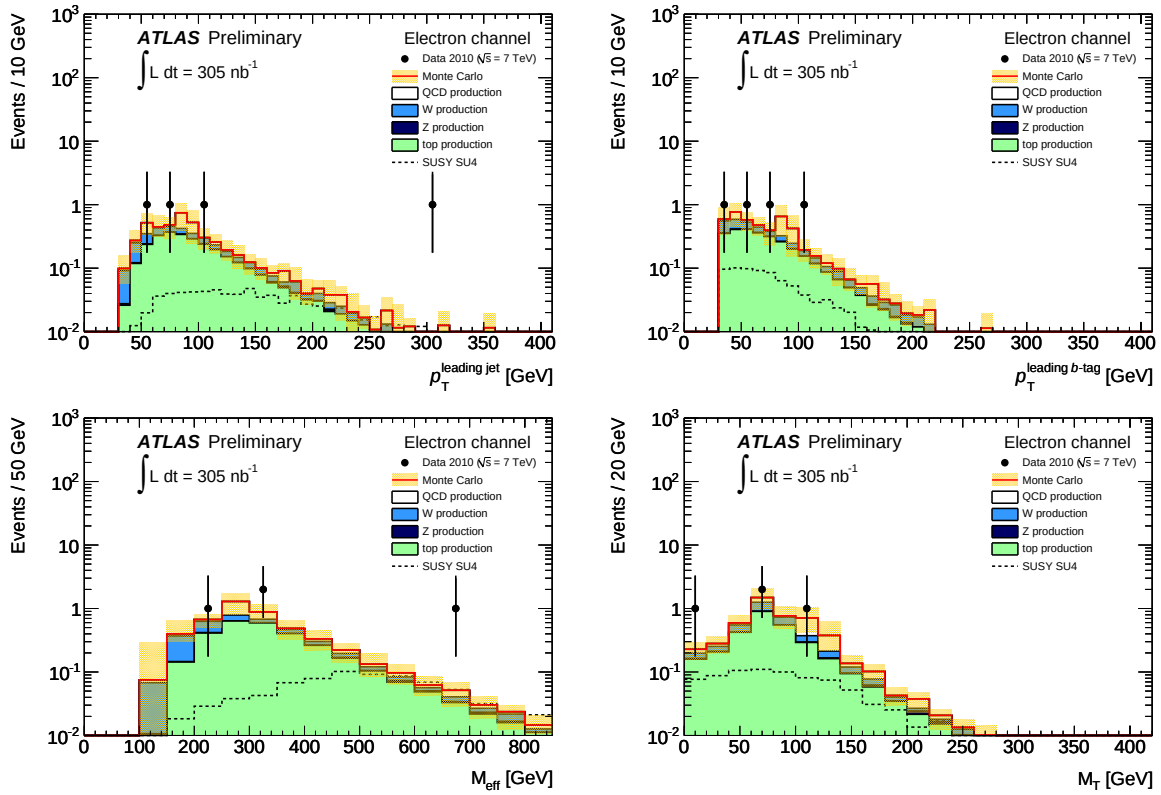

Figure 12: p_{T} of the leading jet (*top left*), p_{T} of the highest SV0 $L/\sigma(L)$ b-tagged jet (*top right*), $\mathrm{M_{eff}}$ (*bottom left*) and transverse mass between the electron and the $E_{\mathrm{T}}^{\mathrm{miss}}$ (*bottom right*) distributions for data and the different Standard Model contributions after the electron channel event selection is applied. The uncertainty band includes statistical and systematic uncertainties. The SU4 supersymmetry benchmark point is also shown.

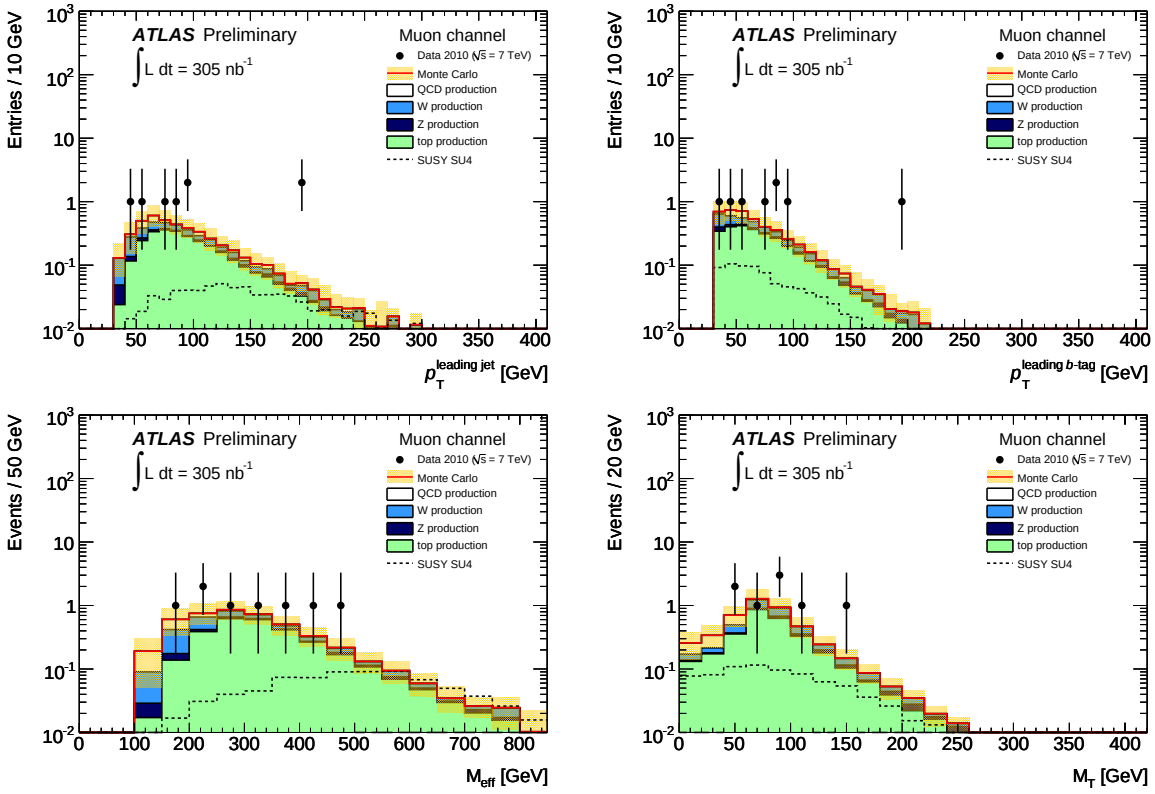

Figure 13: p_{T} of the leading jet (*top left*), p_{T} of the highest SV0 $L/\sigma(L)$ b-tagged jet (*top right*), $\mathrm{M_{eff}}$ (*bottom left*) and transverse mass between the muon and the $E_{\mathrm{T}}^{\mathrm{miss}}$ (*bottom right*) distributions for data and the different Standard Model contributions after the muon channel event selection is applied. The uncertainty band includes statistical and systematic uncertainties. The SU4 supersymmetry benchmark point is also shown.

11 Event Displays of Interesting Events

The events passing the selections for each of the channels have been inspected. One event in the 0-lepton channel containing three *b*-tagged jets, and one event with an isolated electron and a *b*-tagged jet, are presented here. The most relevant properties for the two events, EV1 and EV2, are described in Table 12 and Table 13, respectively.

Name	**EV1**
Run	158975
Event	25441517
M_{eff} [GeV]	432
E_T^{miss} (E_T^{miss} [GeV],ϕ)	(46.1, 1.40)
MetSig [$GeV^{1/2}$]	2.0
1st leading jet (p_T [GeV], η, ϕ [rad]; $L/\sigma(L)$)	(182, 0.30, -1.63; 0)
2nd leading jet (p_T [GeV], η, ϕ [rad]; $L/\sigma(L)$)	(108, 1.15, 1.59; 8.3)
3rd leading jet (p_T [GeV], η, ϕ [rad]; $L/\sigma(L)$)	(54.5, -1.08, 0.58; 19.5)
4th leading jet (p_T [GeV], η, ϕ [rad]; $L/\sigma(L)$)	(42.2, -1.70, -2.8; 12.9)
5th leading jet (p_T [GeV], η, ϕ [rad]; $L/\sigma(L)$)	(21.9, -1.48, -2.34; 0)

Table 12: Details of the event EV1, with three *b*-tagged jets.

Name	**EV2**
Run	159179
Event	5380694
M_{eff} [GeV]	202.3
E_T^{miss} (E_T^{miss} [GeV],ϕ)	(31.3, -2.78)
MetSig [$GeV^{1/2}$]	2.1
Electron (p_T [GeV], η, ϕ [rad]; E_T in isolation cone $\Delta R = 0.2$ [GeV])	(42.3, -0.47, 1.58, 1.9)
M_T [GeV]	60.4
1st leading jet (p_T [GeV], η, ϕ [rad]; $L/\sigma(L)$)	(56.3, 1.57, -0.33; 15.4)
2nd leading jet (p_T [GeV], η, ϕ [rad]; $L/\sigma(L)$)	(39.5, 2.19, -1.86; 0)
3rd leading jet (p_T [GeV], η, ϕ [rad]; $L/\sigma(L)$)	(32.0, 0.72, 2.02; 0)

Table 13: Details of the EV2 event, with one electron and one *b*-tagged jet.

Figure 14 shows different views of EV1. This event contains three *b*-tagged jets, which correspond to three of the four subleading jets present in the event. The highest p_T jet deposits most of the energy ($\sim$ 90%) in the EM calorimeter but several tracks are reconstructed inside the jet cone.

In Figure 15, different views of EV2 are shown. In this case, an electron candidate is observed (see the longitudinal view). The leading jet is *b*-tagged and deposits some energy in the transition region between the central and extended barrel hadron calorimeters. The E_T^{miss} vector

is not aligned to highly energetic jets in the event, and the transverse mass between the electron and the $E_{\mathrm{T}}^{\mathrm{miss}}$ is 60 GeV. This indicates that the event is likely a W+jets or a top candidate.

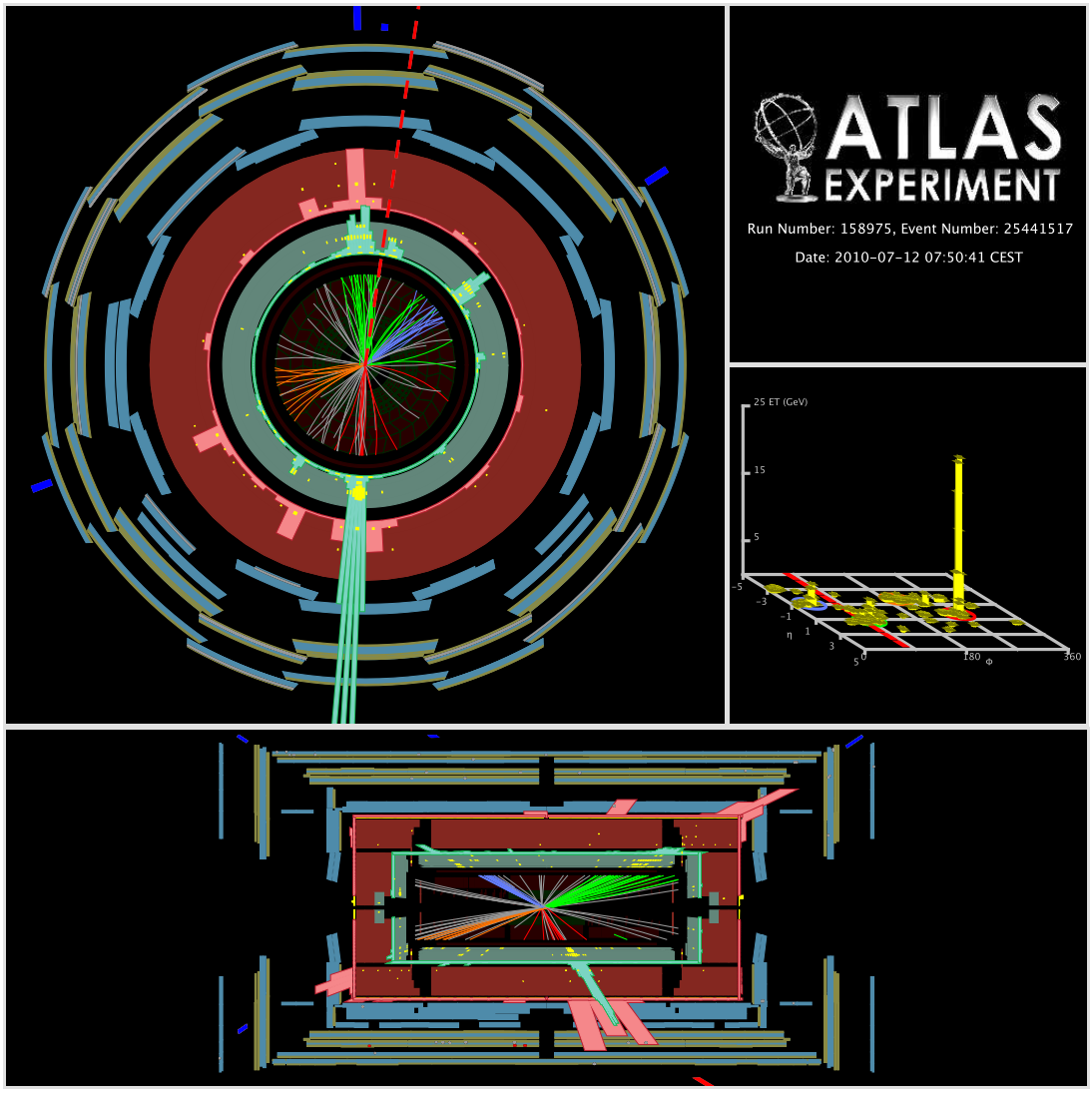

Figure 14: Transverse (*top left*), longitudinal (*bottom*) and lego plot (*top right*) views of the event EV1 (Table 12), with 3 *b*-tagged jets. The energy deposited in the electromagnetic (hadronic) calorimeter is shown in green (red). The direction of the $E_{\mathrm{T}}^{\mathrm{miss}}$ is along the dotted red line. Same colour is applied to all the tracks associated to a particular jet. Muon segments are also shown.

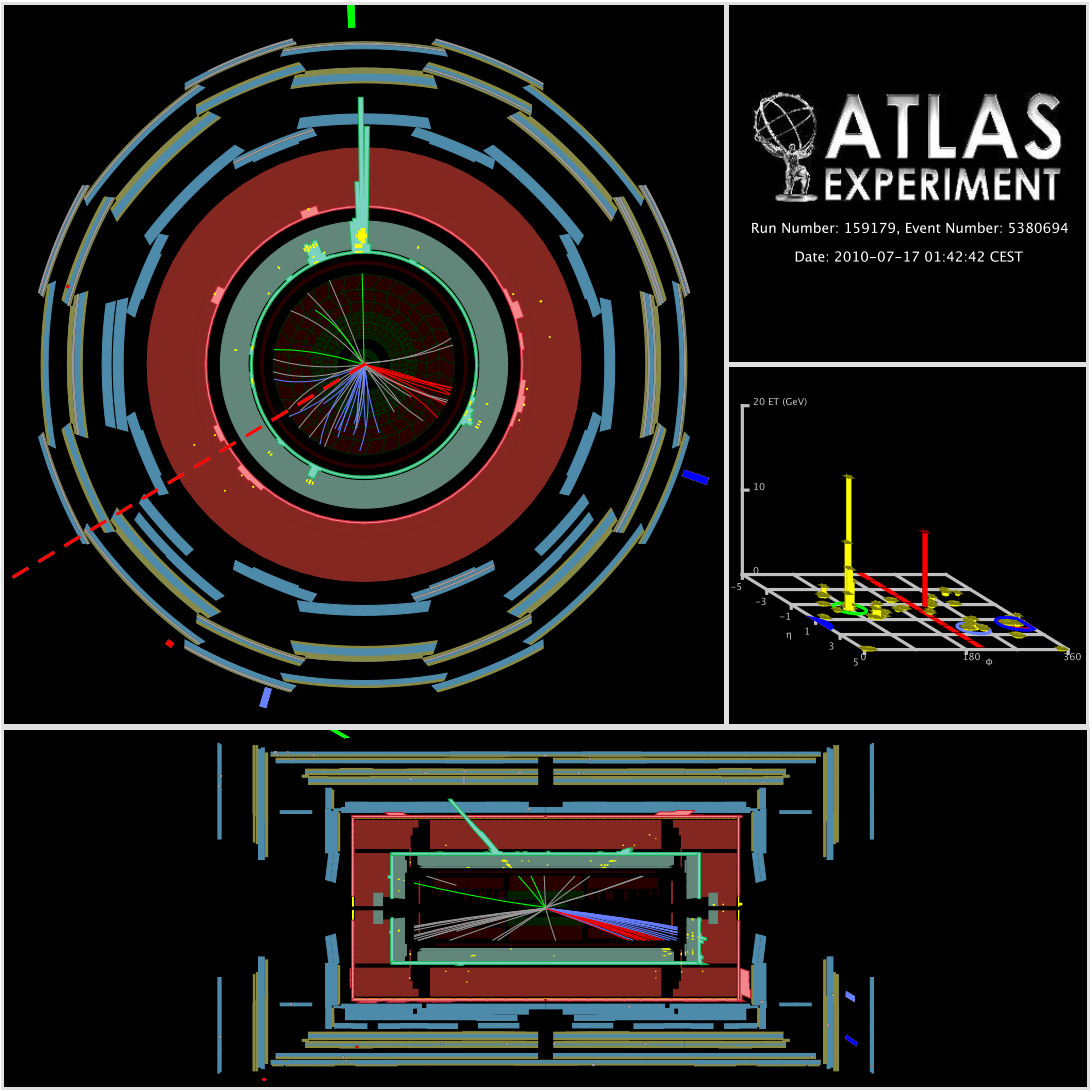

Figure 15: Transverse (*top left*), longitudinal (*bottom*) and lego plot (*top right*) views of the event EV2 (Table 13), with 1 *b*-tagged jet and an isolated electron candidate. The energy deposited in the electromagnetic (hadronic) calorimeter is shown in green (red). The direction of the $E_{\mathrm{T}}^{\mathrm{miss}}$ is along the dotted red line. Same colour is applied to all the tracks associated to a particular jet. Muon segments are also shown.

12 Summary and Conclusion

A study of supersymmetry-sensitive variables in events with missing transverse energy and b-tagged jets has been presented, based on the first 305 nb^{-1} of data collected with the ATLAS detector.

Different jet and lepton multiplicities in the final states have been considered. General good agreement is found between data and Standard Model expectation for several observables before and after b-tagging requirements. These results demonstrate the good level of understanding of the ATLAS performance for jets and tracking.

With larger datasets, more refined techniques to estimate the Standard Model expectation and to reduce the systematic uncertainties will be used, thereby providing increased sensitivity to new physics.

References

[1] Y.A. Golfand and E.P. Likhtman, JETP Lett. **13** (1971) 323–326; A. Neveu and J.H. Schwarz, Nucl. Phys. **B31** (1971) 86–112; A. Neveu and J.H. Schwarz, Phys. Rev. **D4** (1971) 1109–1111; R. Ramond, Phys. Rev. **D3** (1971) 2415–2418; D.V. Volkov and V.P. Akulov, Phys. Lett. **B46** (1973) 109–110; J. Wess and B. Zumino, Phys. Lett. **B49** (1974) 52; J. Wess and B. Zumino, Nucl. Phys. **B70** (1974) 39–50.

[2] L. Evans and P. Bryant, JINST **3** (2008) S08001.

[3] The ATLAS collaboration, Observation of $W \to \ell\nu$ and $Z \to \ell\ell$ production in proton-proton collisions at $\sqrt{s} = 7\,\text{TeV}$ with the ATLAS detector, ATLAS-CONF-2010-044, June 2010.

[4] The ATLAS collaboration, Observation of energetic jets in pp collisions at $\sqrt{s} = 7\,\text{TeV}$ using the ATLAS experiment at the LHC, ATLAS-CONF-2010-043, June 2010.

[5] The ATLAS collaboration, Prospects for supersymmetry discovery based on inclusive searches at a 7 TeV centre-of-mass energy with the ATLAS detector, ATL-PHYS-PUB-2010-010, June 2010.

[6] T. Aaltonen et al., Phys. Rev. Lett. **102** (2009) 121801; Abazov, V. M. et al., Phys. Lett. **B660** (2008) 449–457.

[7] T. Aaltonen et al., Search for the production of scalar bottom quarks in $p\bar{p}$ collisions at $\sqrt{s}$ = 1.96 TeV, 2010; Abazov, V. M. et al., Search for scalar bottom quarks and third-generation leptoquarks in $p\bar{p}$ collisions at $\sqrt{s}$ = 1.96 TeV., 2010.

[8] T. Aaltonen et al., Phys.Rev.Lett. **102** (2009); T. Aaltonen et al., Phys.Rev.Lett. **104** (2010).

[9] The ATLAS collaboration, Early supersymmetry searches in channels with jets and missing transverse momentum with the ATLAS detector, ATLAS-CONF-2010-065, July 2010.

[10] The ATLAS collaboration, Early supersymmetry searches with jets, missing transverse momentum and one or more leptons with the ATLAS Detector, ATLAS-CONF-2010-066, July 2010.

[11] The ATLAS collaboration, JINST **3** (2008) S08003.

[12] The ATLAS collaboration, Luminosity Determination Using the ATLAS Detector, ATLAS-CONF-2010-060, July 2010.

[13] The ATLAS collaboration, Performance of the ATLAS Jet Trigger in the Early $\sqrt{s} = 7$ TeV Data, ATLAS-COM-CONF-2010-047, July 2010.

[14] S. Agostinelli and others, Nucl. Instrum. Meth. **A506** (2003) 250–303.

[15] The ATLAS Collaboration, The ATLAS Simulation Infrastructure, Submitted to Eur. Phys. J. C; arXiv:1005.4568v1, May 2010.

[16] T. Sjostrand, and S. Mrenna and P. Skands, JHEP **05** (2006) 026.

[17] The ATLAS collaboration, ATLAS Monte Carlo tunes for MC09, ATL-PHYS-PUB-2010-002, 2010.

[18] A. Sherstnev and R.S. Thorne, Eur. Phys. J. **C55** (2008) 553–575.

[19] M. Mangano and others, JHEP **07** (2003) 001.

[20] G. Corcella and others, JHEP **01** (2001) 010; G. Corcella and others, *HERWIG 6.5 release note*, hep-ph/0210213, 2002.

[21] J. Butterworth, J. Forshaw and M. Seymour, Z. Phys. **C72** (1996) 637–646.

[22] D. Stump and others, JHEP **10** (2003) 046.

[23] C. Anastasiou, L.J. Dixon, K. Melnikov, and F. Petriello, Phys. Rev. **D69** (2004) 094008.

[24] S. Frixione and B.R. Webber, The MC@NLO 3.2 event generator, hep-ph/0601192, 2006.

[25] S. Moch and P. Uwer, Nucl. Phys. Proc. Suppl. **183** (2008) 75–80.

[26] M. Bahr and others, Eur. Phys. J. **C58** (2008) 639–707; M. Bahr and others, Herwig++ 2.3 release note, arXiv:0812.0529, 2008.

[27] F.E. Paige, S.D. Protopopescu, H. Baer, and X. Tata, ISAJET 7.69: A Monte Carlo event generator for p p, anti-p p, and e+ e- reactions, hep-ph/0312045, 2003.

[28] W. Beenakker, R. Hopker and M. Spira, PROSPINO: A program for the production of supersymmetric particles In next-to-leading order QCD, hep-ph/9611232, 1996; *PROSPINO2*, `http://www.ph.ed.ac.uk/~tplehn/prospino/`.

[29] The ATLAS collaboration, Performance of the ATLAS Secondary Vertex b-tagging Algorithm in 7 TeV Collision Data, ATLAS-CONF-2010-042, June 2010.

[30] M. Cacciari, G.P. Salam and G. Soyez, JHEP **04** (2008) 063.

[31] The ATLAS collaboration, Jet energy scale and its systematic uncertainty in ATLAS for jets produced in proton-proton collisions at $\sqrt{s} = 7$ TeV, ATLAS-CONF-2010-056, June 2010.

[32] The ATLAS collaboration, Data-quality requirements and event cleaning for jets and missing transverse energy reconstruction with the ATLAS detector in proton-proton collisions at a center-of-mass energy of $\sqrt{s} = 7$ TeV, ATLAS-CONF-2010-038, July 2010.

[33] The ATLAS collaboration, Performance of the missing transverse energy reconstruction in minimum bias collisions at center-of-mass energy of $\sqrt{s} = 7$ TeV with the ATLAS detector, ATLAS-CONF-2010-057, 2010.

[34] The ATLAS collaboration, Expected performance of the ATLAS experiment – detector, trigger and physics, page 1589-1616, arXiv:0901.0512, 2009.

[35] The ATLAS Collaboration, Discovery Potential for Supersymmetry with b-jet Final States with the ATLAS detector, ATL-PHYS-PUB-2009-075, May 2009.

[36] The CMS collaboration, Inclusive b-jet production in pp collisions at $\sqrt{s} = 7$ TeV, CMS PAS BPH-10-009, July 2010.